### Title

Protection of Molecular Microcrystals by Encapsulation under Single-Layer Graphene.




### Journal

ACS omega, 3(7)

### ISSN

2470-1343



### Authors

Li, Wangxiang

Tierce, Nathan T

Bekyarova, Elena

et al.



### Publication Date

2018-07-01

### DOI

10.1021/acsomega.8b00872

Peer reviewed

ACS OMEGA

Article

Cite This: ACS Omega 2018, 3, 8129−8134

# Protection of Molecular Microcrystals by Encapsulation under Single-Layer Graphene

Wangxiang Li,[†,‡] Nathan T. Tierce,[†] Elena Bekyarova,*[,†,‡] and Christopher J. Bardeen*[,†]

[†]Department of Chemistry, University of California, 501 Big Springs Road, Riverside, California 92521, United States

[‡]Center for Nanoscale Science and Engineering, University of California, 900 University Avenue, Riverside, California 92521, United States

Supporting Information

**ABSTRACT:** Microcrystals composed of the conjugated organic molecule perylene can be encapsulated beneath single-layer graphene using mild conditions. Scanning electron and atomic force microscopy images show that the graphene exists as a conformal coating on top of the crystal. Raman spectroscopy indicates that the graphene is only slightly perturbed by the underlying crystal, probably due to strain. The graphene layer provides complete protection from a variety of solvents and prevents sublimation of the crystal at elevated temperatures. Time-resolved photoluminescence measurements do not detect any quenching of the perylene emission by the graphene layer, although nonradiative energy transfer within a few nanometers of the crystal−graphene interface cannot be ruled out. The ability to encapsulate samples on a substrate under a graphene monolayer may provide a new way to access and interact with the organic crystal under ambient conditions.

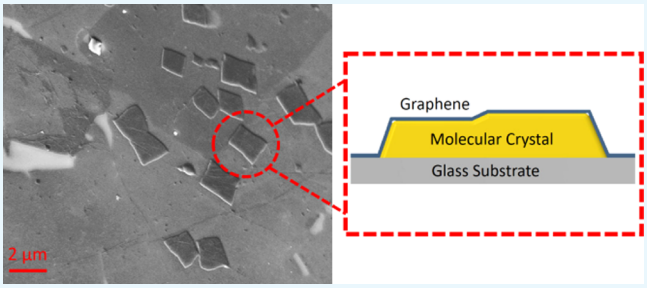


## INTRODUCTION

Two-dimensional (2D) materials have attracted the attention of researchers due to their novel physical properties, such as ultrahigh carrier mobilities, thermal conductivity, and mechanical toughness.[1,2] As a prototypical 2D material, graphene has been the subject of extensive study. This atomically thin membrane allows photons, electrons, and even protons to pass through but is impermeable to other chemical species, even those as small as atomic helium.[3−6] This impermeability has raised interest in the application of graphene as a protective coating, e.g., to prevent corrosion of an underlying metal.[7] Typically, these coatings consist of many overlapping flakes of graphene such that there is not complete encapsulation, but rather a slowing of the diffusion as the reactive species navigate around the sheets.

Reports of complete encapsulation of objects using graphene are relatively rare. Several groups have used graphene to encapsulate liquid samples for electron microscopy experiments,[8−10] but these methods are challenging to implement, since they rely on using a pair of sheets to sandwich a liquid droplet. Ideally, one would develop a method whereby individual microscale objects on a solid support can be "shrink-wrapped" by an atomically thin sheet of graphene, making them impervious to chemical attack while still allowing optical and/or electrical access. The encapsulation of metal nanowires between graphene and plastic using hot lamination suggests that such an approach is feasible.[11] However, a more general encapsulation method using milder conditions on an inorganic surface would be desirable for organics. Ideally, graphene would make an atomically tight seal with an inert substrate such as glass.

Crystals composed of conjugated organic molecules make a good test system for graphene encapsulation. These crystals possess interesting electronic and photophysical properties,[12] with those based on polycyclic aromatic hydrocarbons being of special interest.[13,14] They tend to be sensitive to the presence of impurities like $O_2$ or organic contaminants, which can degrade their electronic properties. Organic crystals also dissolve when exposed to organic solvents and sublime when exposed to high vacuum or elevated temperatures. Current protection strategies include isolating them under vacuum or an inert atmosphere and encapsulating them between glass plates sealed with epoxy. In both cases, the crystal becomes inaccessible to electrical or optical probes that require close sample contact like scanning probe microscopies.

This study describes a method to encapsulate single microcrystals composed of the prototypical conjugated organic molecule perylene (PER) beneath monolayer graphene. While graphene has been used previously as a substrate for organic crystal growth,[15,16] its use as an encapsulation layer is relatively unexplored. We used PER as a test crystal because its $\alpha$-polymorph tends to grow in a signature square shape and produces a strong visible photoluminescence (PL) signal. These characteristics allow us to optically detect the presence

Received: May 1, 2018
Accepted: June 21, 2018
Published: July 20, 2018

  

DOI: 10.1021/acsomega.8b00872
ACS Omega 2018, 3, 8129−8134

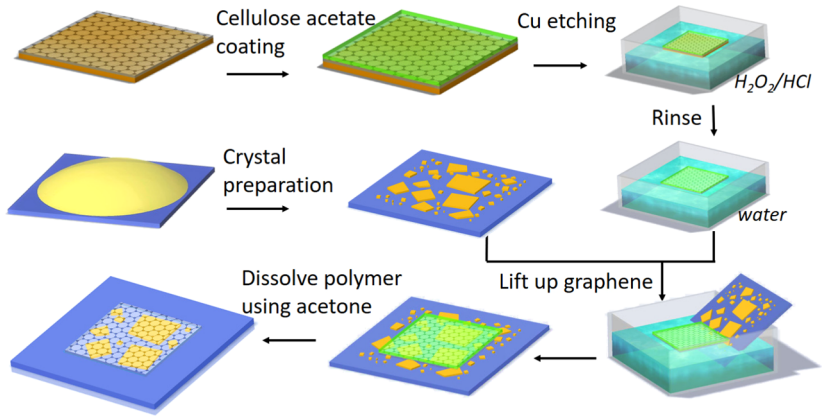


**Figure 1.** Schematic illustration of the graphene encapsulation process for molecular microcrystals.

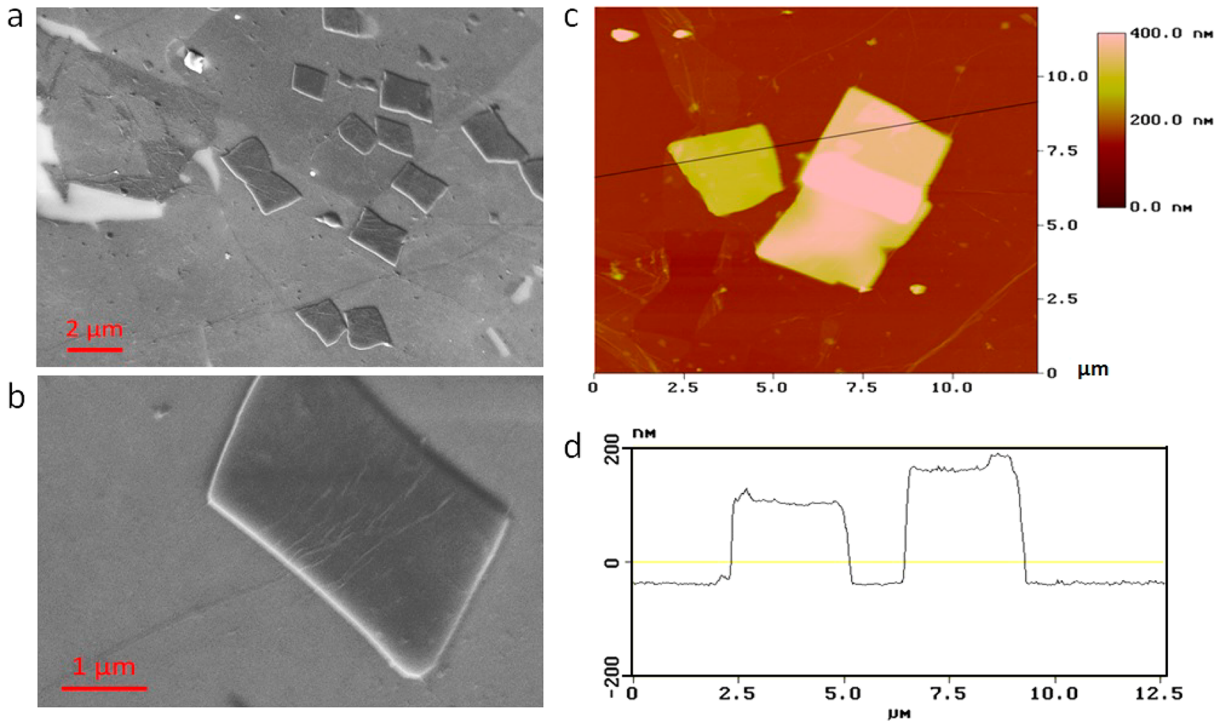


**Figure 2.** (a,b) SEM images of graphene covered PER crystals on glass with low and high magnification. Note that the continuation of the graphene wrinkles from the substrate surface across the PER crystal in (b) provides visual evidence the encapsulation. (c) AFM image of graphene covered perylene crystals with (d) cross section analysis. The typical diameter of the covered crystals is around 2 $\mu$m and the thickness is around 150 nm.

of these crystals underneath graphene sheet and assess how they respond to solvent exposure and elevated temperatures. The effect of graphene layer on the PER excimer dynamics can be measured by the photoluminescence (PL) decay. Our results demonstrate that a 2D monolayer can completely encapsulate a molecular crystal and turn it into a sample that is robust with respect to air and solvent exposure as well as high temperatures. This new capability to protect fragile crystals should open the door to routine characterization of these fragile semiconductors using microscopy techniques with nanometer resolution,[17] as well as new ways to interface them with other materials.

## RESULTS AND DISCUSSION

The procedure for coating PER microcrystals with graphene is outlined in Figure 1 and described in detail in the Supporting Information.[18] Briefly, large-area single-layer graphene sheets grown on a Cu foil substrate by chemical vapor deposition are purchased from a commercial vendor. A cellulose acetate polymer layer with a thickness of several microns is spin-cast on top of the graphene and then the Cu is dissolved in a solution of $HCl/H_2O_2$. After the Cu layer is completely etched away, the solution is replaced with clean water and the graphene−polymer layer is floated on the water surface. A glass substrate, on top of which random PER microcrystals have been grown by solvent evaporation, is then dipped into the water and positioned underneath the supported graphene. It is then lifted up with the graphene layer on top. The end result is a sample consisting of the glass substrate with PER crystals underneath a blanket of graphene with the polymer support layer on top. The final step involves dissolving the polymer-supporting layer by rinsing with acetone. The presence of graphene can be readily discerned by its modified reflectivity, and it is easy to see breaks and holes in the coating



DOI: 10.1021/acsomega.8b00872
ACS Omega 2018, 3, 8129−8134

(Supporting Information). Most of the original PER microcrystals are dissolved by the acetone rinse, but in regions containing intact graphene sheets, the underlying PER crystals can be readily imaged using optical, electron, and atomic force microscopy (AFM) methods.

Figure 2a,b shows scanning electron microscopy (SEM) images of PER crystals under single-layer graphene. We note that this imaging was done without a metal coating, since graphene's high conductivity prevents charging of the low-conductivity organic crystal and enables electron microscopy to be performed under vacuum without further treatment. In Figure 2b, one can see a wrinkle in the graphene sheet that continues from the substrate across the edge and onto the crystal surface. This wrinkling was an exception; in almost all other cases, close adhesion of the graphene sheet to the crystal and glass surfaces led to a conformal coating. There is no sign of "tenting", in which the graphene sheet detaches from the surface and is free floating between the crystal and the surface. Tenting was observed for taller or more irregularly shaped objects such as inorganic dust particles adhered to the substrate surface (Supporting Information, Figure S1). The conformal nature of the encapsulation was confirmed by atomic force microscopy (AFM). Figure 2c shows an AFM image of a pair of encapsulated crystals, while Figure 2d shows the height profile of the crystals taken along the axis shown in Figure 2c. The profile image in Figure 2d illustrates the size variation in the PER crystal plates, whose thickness typically ranged from 100 to 200 nm. The images also show how the graphene conforms to the crystal, following the sharp crystal edge down to the substrate surface.

Raman spectroscopy is a standard method to evaluate the quality of graphene layers.[19] Figure 3 compares the Raman spectra of graphene on top of both the $SiO_2$ substrate and a PER crystal. Both Raman spectra show the signature G peak in the range of 1580−1590 $cm^{-1}$ and the 2D peak at around 2600 $cm^{-1}$. The G/2D peak intensity ratio ($I_G/I_{2D} < 1$) indicates monolayer coverage. The small amplitude of the D peak at 1300 $cm^{-1}$ for the graphene layer on $SiO_2$ shows that it is largely free of defects.[19] The Raman spectrum on the PER does not appear to have an enhanced D peak intensity, suggesting that it has the same low defect level, but two additional peaks at 1297 and 1369 $cm^{-1}$ also appear on top of this feature. These peaks are also prominent in the Raman spectrum of PER microcrystals (Supporting Information, Figures S3 and S4) and originate from the PER double-bond stretches.[20,21] It is interesting that the PER and graphene Raman signals are of comparable strength. The 780 nm excitation wavelength is far from the PER absorption at 500 nm but still resonant with the semimetallic graphene. The very strong Raman signal of the delocalized electrons in graphene more than compensates for its lower mass fraction in this sample.

The exact positions of the G and 2D peaks can provide information about the state of the graphene. In pristine graphene, the G peak is located at 1580 $cm^{-1}$. The G peak of our graphene on glass is located at 1589 $cm^{-1}$, consistent with doping by exposure to ambient $O_2$ after preparation in air.[22,23] The Raman spectrum of graphene on top of PER exhibits a slight downshift in both the G (−8 $cm^{-1}$) and 2D (−18 $cm^{-1}$) peaks relative to those of graphene on $SiO_2$. Larger PER crystals resulted in larger downshifts of the Raman peaks, with the largest crystal shifting the G peak all the way to 1570 $cm^{-1}$ (Supporting Information, Figure S5). These larger G peak shifts were accompanied by larger 2D peak shifts up to 25

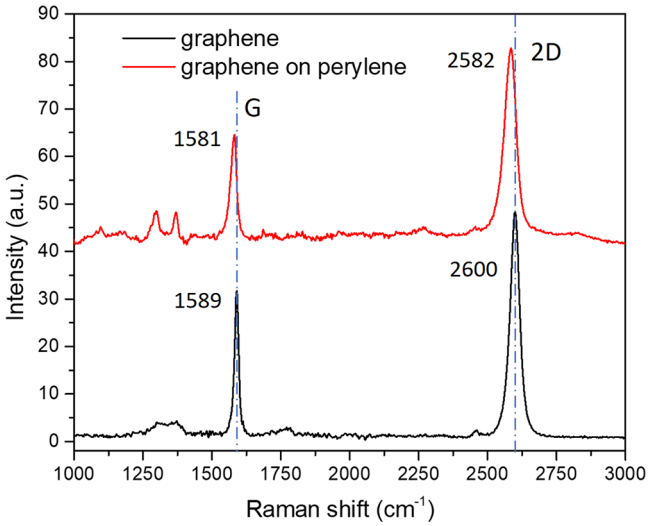


**Figure 3.** Raman spectra of graphene films on glass substrate (black) and on top of a PER crystal (red). The excitation wavelength is 780 nm. Both spectra show the characteristic graphene peaks: G and 2D peaks. Red shifts for both G (−8 $cm^{-1}$) and 2D (−18 $cm^{-1}$) peaks are observed for the graphene on top of the PER crystal, along with additional peaks at 1297 and 1369 $cm^{-1}$ from the PER.

$cm^{-1}$. These shifts were robust with respect to background subtraction and data reduction methods.

There are several factors that can lead to shifting Raman peaks in graphene. Both n- and p-doping typically lead to an upshift of the G-band Raman frequencies,[24] but this is the opposite of what we observe. Given that the graphene sheet is already p-doped due to oxygen exposure, one possibility is that the organic crystal removes charge carriers or $O_2$ from the graphene sheets. Such an undoping process would be expected to shift the G peak back to 1580 $cm^{-1}$, but not below. The fact that we observe shifts of both G and 2D peaks to positions well below those of pristine graphene suggests that the more likely culprit is strain as the graphene stretches to accommodate the underlying crystal. The shifts in both G and 2D peaks are consistent with a strain of approximately 0.5% on a crystal with thickness of about 150 nm, based on previous measurements on stretched sheets of graphene.[25,26] This stretching would explain the conformal nature of the coating deduced from the images in Figure 2 and is consistent with the "shrink-wrap" concept. The Raman shifts provide evidence that the interaction of graphene with the underlying crystal induces a slight stretching but no dramatic changes in the electronic structure or defect density. It is possible, however, that the graphene sheet experiences higher localized strain at the crystal edges, which could lead to larger effects on its electronic properties.[27]

PER is a highly soluble small molecule that sublimes easily, but the graphene−glass encapsulation stabilizes the microcrystals under a variety of conditions. The samples can be left on the benchtop, under room light, for days without any change in PL brightness. The encapsulated crystals survive immersion in a variety of organic solvents (acetone, tetrahydrofuran (THF), toluene, methanol, and methylene chloride) for more than 1 day without change. Unprotected crystals dissolved within 1 min under the same conditions. When heated to 100 °C in air, unprotected crystals sublimed within 40 min, but encapsulated crystals resisted sublimation up to 250 °C, close to PER's melting point of 278 °C. At



DOI: 10.1021/acsomega.8b00872
ACS Omega 2018, 3, 8129−8134

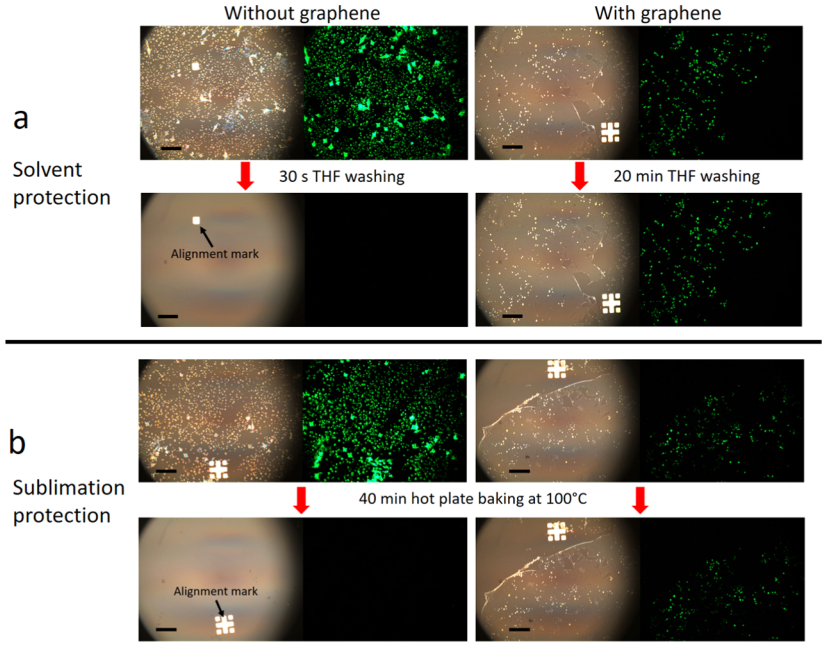


**Figure 4.** Transmitted and fluorescence microscopy images showing the effect of monolayer graphene encapsulation on the stability of PER microcrystals. The substrates are standard microscope slides with gold alignment marks. (a) Before and after washing with THF: 30 s washing resulted in 100% dissolution of unprotected crystals, while 20 min THF washing had no effect on protected crystals. (b) Before and after heating at 100 °C for 40 min: the unprotected crystals sublime completely, but the protected crystals remain intact. The scale bar is 50 $\mu$m.

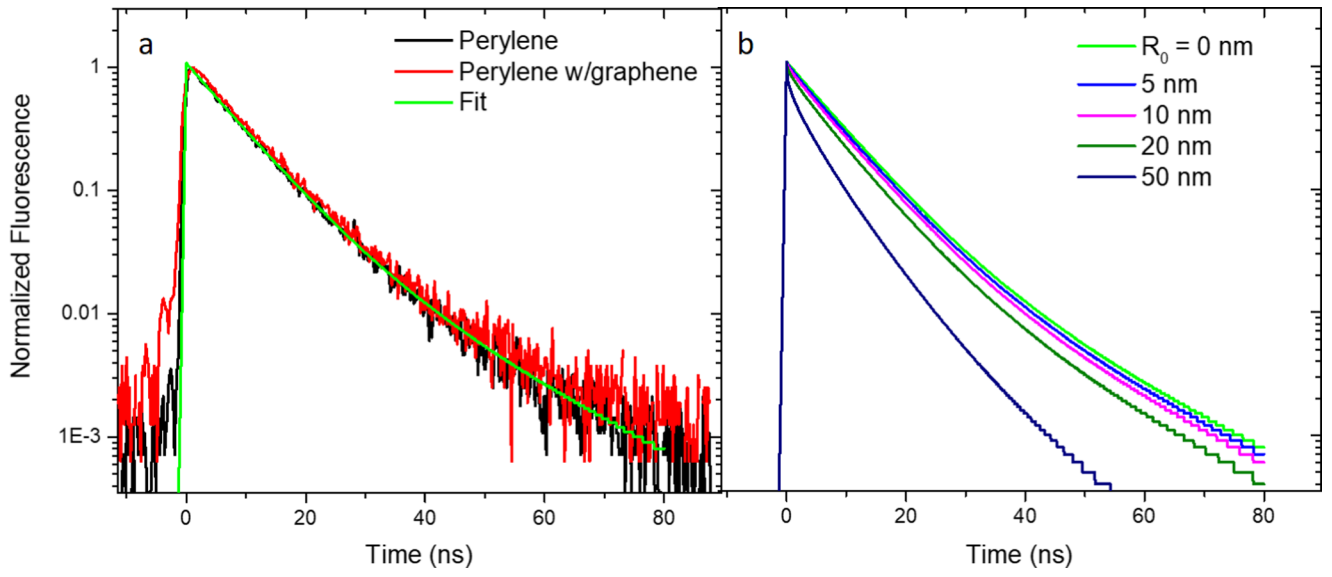


**Figure 5.** (a) Time-resolved photoluminescence of PER (black) and graphene-coated PER crystals (red) excited at 400 nm. The lifetime of crystalline PER is unchanged when coated with graphene. (b) Calculated PL decays for different $R_0$ values for the graphene quenching function described in the text for a 150 nm thick crystal. When $R_0 \geq 20$ nm, there is a notable deviation from the intrinsic PER decay.

higher temperatures, the PER melted and then rapidly disappeared. Comparisons of graphene-protected and unprotected PER crystals after exposure to solvent and elevated temperatures are shown in Figure 4. The fact that the graphene sheet provides protection from solvent dissolution and sublimation is evidence that the graphene makes an atomically tight seal with the glass substrate that completely prevents penetration by solvent molecules as well as escape of the PER molecules at elevated temperatures. The encapsulation only failed when the PER itself could diffuse (after melting) or if the graphene did not remain intact. Objects with large height variations tended to rupture the graphene (Supporting Information, Figure S1), allowing solvent penetration and dissolution.

Graphene is not a completely inert coating, since it is a semimetal that may be expected to affect the electronic properties of the crystal. For example, it is likely to quench molecular excitons due to either energy[28−30] or electron transfer.[31,32] Although the precise distance dependence and mechanism of the PL quenching remain a subject of active investigation, the characteristic distance has been estimated to extend up to 60 nm.[33] To investigate the possibility of PL quenching, the excimer lifetime of the PER microcrystals was measured by time-resolved PL experiments. The PL spectra



DOI: 10.1021/acsomega.8b00872
ACS Omega 2018, 3, 8129−8134

with and without graphene encapsulation are similar, showing the Y (550 nm) and E (600 nm) peaks as observed in $\alpha$-PER crystals (Supporting Information, Figure S6).[34] The Y peak in our samples is more pronounced than for typical bulk crystals,[35,36] as often observed for nanocrystalline samples with higher defect densities.[37,38] The PL decays of the two samples are identical, as shown in Figure 5a, although the signal level of the encapsulated sample is considerably lower due to the scarcity of surviving crystals. We note that these PER crystals, grown from solution, have a more rapid PL decay than sublimation-grown crystals from zone-refined PER.[34] It is likely that the PL decay is accelerated by the presence of defects in our solution-grown PER crystals. But the important point is that there is no detectable PL quenching by the graphene overlayer.

Even though there is no detectable change in the PL decay, it is likely that excitons near the top surface of the crystal, close to the graphene layer, are quenched. We can place an approximate upper bound on the quenching radius of the graphene using a simple model to analyze the PL decay. We assume an average crystal thickness of 150 nm and that the quenching rate of the 2D graphene sheet is given by $k_{\text{quench}} = \frac{R_0^4}{R^4}$, where $R_0$ is the critical distance for a dipole interacting with a 2D energy acceptor.[39,40] The experimental PL decay is parameterized as a biexponential with amplitudes $A_1 = 0.925$ and $A_2 = 0.075$ and decay times $\tau_1 = 7.5$ ns and $\tau_2 = 17.4$ ns. The functional form of the PL decay is then the product of the intrinsic biexponential and the quenching term

$$\text{PL}(t) \approx [A_1\, e^{-(t/\tau_1)} + A_2\, e^{-(t/\tau_1)}] \times e^{-k_{\text{quench}}t} \quad (1)$$

In Figure 5b, we compare the PL decays calculated assuming different values of $R_0$ and summing up the contributions of eq 1 for all $R$ values in a 150 nm thick crystal. For $R_0 = 20$ nm, the deviation of the calculated decay from the intrinsic decay should be observable. Similar results are obtained for crystal thicknesses of 100 and 200 nm (Supporting Information, Figure S8). The fact that this deviation is not experimentally observed allows us to estimate a conservative upper bound of $R_0 \leq 20$ nm. This limit is consistent with a value of $R_0 \sim 10$ nm extracted from distance-dependent quenching of a rhodamine dye on top of graphene[41] and suggests that only excitons in the top layer of the PER crystal are quenched by the graphene.

The ability to observe electronic perturbations due to graphene will depend on the nature of the organic sample. In PER, the effect of the graphene quenching may be more easily observed for thinner crystals that have a larger fraction of molecules close to the surface or for higher-quality crystals that can support longer exciton diffusion lengths. Different types of crystals may have significant electronic interactions with the graphene layer, for example, charge transfer. Surface-sensitive measurements of the electronic properties will likely be sensitive to the graphene–organic interaction. A second issue is that the method of preparation exposes the sample to water during the graphene lift up. While the graphene clearly prevents access by molecules outside the encapsulation layer, it can also trap impurities or water molecules inside the layer with the crystal. The stability of the graphene-encapsulated sample will allow such effects to be studied for samples that might be sensitive to the presence of such extrinsic chemical species.

## CONCLUSIONS

In summary, we have demonstrated that it is possible to create robust molecular crystal samples that are fully encapsulated beneath a monolayer of graphene. The graphene layer provides complete protection from a variety of solvents and prevents sublimation of the crystal at elevated temperatures. Raman measurements show that the graphene layer is only slightly perturbed by the underlying crystal, while time-resolved PL measurements show no detectable quenching of the PER excimers by the graphene. The fact that graphene can make a tight seal with glass suggests that this method can be extended to other 2D encapsulating materials, for example, hexagonal boron nitride, whose large band gap would preclude any possibility of energy transfer. This technique may also make it possible to interface organic crystals with other materials that have incompatible processing conditions like metal electrodes created by focused ion beam deposition under high vacuum or polymers cast from solvents that would normally dissolve the crystal. The ability to keep organic solid crystals intact under such processing conditions raises the possibility of fabricating an organic–organic heterojunction to study energy transfer and/or charge transfer across a 2D membrane.

## ASSOCIATED CONTENT

### Supporting Information

The Supporting Information is available free of charge on the ACS Publications website at DOI: 10.1021/acsomega.8b00872.

Experimental procedures, Raman data work-up, SEM images, PL spectra, and linear PL time trace of PER (PDF)

## AUTHOR INFORMATION


### Corresponding Authors

*E-mail: elena.bekyarova@ucr.edu (E.B.).
*E-mail: christopher.bardeen@ucr.edu (C.J.B.).

### ORCID

Christopher J. Bardeen: 0000-0002-5755-9476


### Notes

The authors declare no competing financial interest.

## ACKNOWLEDGMENTS

This study was supported by the National Science Foundation grants DMR-1508099 (C.J.B.) and DMR-1305724 (E.B.).

## REFERENCES


(1) Novoselov, K. S.; Fal'ko, V. I.; Colombo, L.; Gellert, P. R.; Schwab, M. G.; Kim, K. A Roadmap for Graphene. *Nature* **2012**, *490*, 192–200.

(2) Butler, S. Z.; Hollen, S. M.; Cao, L.; Cui, Y.; Gupta, J. A.; Gutierrez, H. R.; Heinz, T. F.; Hong, S. S.; Huang, J.; Ismach, A. F.; Johnston-Halperin, E.; Kuno, M.; Plashnitsa, V. V.; Robinson, R. D.; Ruoff, R. S.; Salahuddin, S.; Shan, J.; Shi, L.; Spencer, M. G.; Terrones, M.; Windl, W.; Goldberger, J. E. Progress, Challenges, and Opportunities in Two-Dimensional Materials Beyond Graphene. *ACS Nano* **2013**, *7*, 2898–2926.

(3) Bunch, J. S.; Verbridge, S. S.; Alden, J. S.; van der Zande, A. M.; Parpia, J. M.; Craighead, H. G.; McEuen, P. L. Impermeable Atomic Membranes from Graphene Sheets. *Nano Lett.* **2008**, *8*, 2458–2462.

(4) Berry, V. Impermeability of Graphene and its Applications. *Carbon* **2013**, *62*, 1–10.

(5) Hu, S.; Lozada-Hidalgo, M.; Wang, F. C.; Mishchenko, A.; Schedin, F.; Nair, R. R.; Hill, E. W.; Boukhvalov, D. W.; Katsnelson,




DOI: 10.1021/acsomega.8b00872
*ACS Omega* 2018, 3, 8129–8134

M. I.; Dryfe, R. A. W.; Grigorieva, I. V.; Wu, H. A.; Geim, A. K. Proton Transport through One-Atom-Thick Crystals. *Nature* **2014**, *516*, 227−230.
(6) Kaplan, A.; Yuan, Z.; Benck, J. D.; Rajan, A. G.; Chu, X. S.; Wang, Q. H.; Strano, M. S. Current and Future Directions in Electron Transfer Chemistry of Graphene. *Chem. Soc. Rev.* **2017**, *46*, 4530−4571.
(7) Nine, M. J.; Cole, M. A.; Tran, D. N. H.; Losic, D. Graphene: a Multipurpose Material for Protective Coatings. *J. Mater. Chem. A* **2015**, *3*, 12580−12602.
(8) Mohanty, N.; Fahrenholtz, M.; Nagaraja, A.; Boyle, D.; Berry, V. Impermeable Graphenic Encasement of Bacteria. *Nano Lett.* **2011**, *11*, 1270−1275.
(9) Yuk, J. M.; Park, J.; Ercius, P.; Kim, K.; Hellebusch, D. J.; Crommie, M. F.; Lee, J. Y.; Zettl, A.; Alivisatos, A. P. High-Resolution EM of Colloidal Nanocrystal Growth Using Graphene Liquid Cells. *Science* **2012**, *336*, 61−64.
(10) Chen, Q.; Smith, J. M.; Park, J.; Kim, K.; Ho, D.; Rasool, H. I.; Zettl, A.; Alivisatos, A. P. 3D Motion of DNA-Au Nanoconjugates in Graphene Liquid Cell Electron Microscopy. *Nano Lett.* **2013**, *13*, 4556−4561.
(11) Deng, B.; Hsu, P.-C.; Chen, G.; Chandrashekar, B. N.; Liao, L.; Ayitimuda, Z.; Wu, J.; Guo, Y.; Lin, L.; Zhou, Y.; Aisijiang, M.; Xie, Q.; Cui, Y.; Liu, Z.; Peng, H. Roll-to-Roll Encapsulation of Metal Nanowires between Graphene and Plastic Substrate for High-Performance Flexible Transparent Electrodes. *Nano Lett.* **2015**, *15*, 4206−4213.
(12) Podzorov, V. Organic Single Crystals. *MRS Bull.* **2013**, *38*, 15−24.
(13) Anthony, J. E. The Larger Acenes: Versatile Organic Semiconductors. *Angew. Chem., Int. Ed.* **2008**, *47*, 452−483.
(14) Rieger, R.; Mullen, K. Forever Young: Polycyclic Aromatic Hydrocarbons as Model Cases for Structural and Optical Studies. *J. Phys. Org. Chem.* **2010**, *23*, 315−325.
(15) Lee, C.-H.; Schiros, T.; Santos, E. J. G.; Kim, B.; Yager, K. G.; Kang, S. J.; Lee, S.; Yu, J.; Watanabe, K.; Taniguchi, T.; Hone, J.; Kaxiras, E.; Nuckolls, C.; Kim, P. Epitaxial Growth of Molecular Crystals on van der Waals Substrates for High-Performance Organic Electronics. *Adv. Mater.* **2014**, *26*, 2812−2817.
(16) Zhang, Y.; Diao, Y.; Lee, H.; Mirabito, T. J.; Johnson, R. W.; Puodziukynaite, E.; John, J.; Carter, K. R.; Emrick, T.; Mannsfeld, S. C. B.; Briseno, A. L. Intrinsic and Extrinsic Parameters for Controlling the Growth of Organic Single-Crystalline Nanopillars in Photovoltaics. *Nano Lett.* **2014**, *14*, 5547−5554.
(17) Schuck, P. J.; Weber-Bargioni, A.; Ashby, P. D.; Ogletree, D. F.; Schwartzberg, A.; Cabrini, S. Life Beyond Diffraction: Opening New Routes to Materials Characterization with Next-Generation Near-Field Approaches. *Adv. Funct. Mater.* **2013**, *23*, 2539−2553.
(18) Chen, M.; Li, G.; Li, W.; Stekovic, D.; Arkook, B.; Itkis, M. E.; Pekker, A.; Bekyarova, E.; Haddon, R. C. Large-Scale Cellulose-Assisted Transfer of Graphene Toward Industrial Applications. *Carbon* **2016**, *110*, 286−291.
(19) Ferrari, A. C.; Basko, D. M. Raman Spectroscopy as a Versatile Tool for Studying the Properties of Graphene. *Nat. Nanotechnol.* **2013**, *8*, 235−246.
(20) Matsunuma, S.; Akamatsu, N.; Kamisuki, T.; Adachi, Y.; Maeda, S.; Hirose, C. $S_n$<− $S_1$ and $S_1$−>$S_0$ Resonance CARS Spectra of Perylene in the $S_1$ State. *J. Chem. Phys.* **1988**, *88*, 2956−2961.
(21) Shinohara, H.; Yamakita, Y.; Ohno, K. Raman Spectra of Polycyclic Aromatic Hydrocarbons. Comparison of Calculated Raman Intensity Distributions with Observed Spectra for Naphthalene, Anthracene, Pyrene, and Perylene. *J. Mol. Struct.* **1998**, *442*, 221−234.
(22) Ryu, S.; Liu, L.; Berciaud, S.; Yu, Y. J.; Liu, H.; Kim, P.; Flynn, G. W.; Brus, L. E. Atmospheric Oxygen Binding and Hole Doping in Deformed Graphene on a $SiO_2$ Substrate. *Nano Lett.* **2010**, *10*, 4944−4951.
(23) Piazza, A.; Giannazzo, F.; Buscarino, G.; Fisichella, G.; Magna, A. L.; Roccaforte, F.; Cannas, M.; Gelardi, F. M.; Agnello, S. Effect of Air on Oxygen p-Doped Graphene on $SiO_2$. *Phys. Status Solidi A* **2016**, *213*, 2341−2344.
(24) Das, A.; Pisana, S.; Chakraborty, B.; Piscanec, S.; Saha, S. K.; Waghmare, U. V.; Novoselov, K. S.; Krishnamurthy, H. R.; Geim, A. K.; Ferrari, A. C.; Sood, A. K. Monitoring Dopants by Raman Scattering in an Electrochemically Top-Gated Graphene Transistor. *Nat. Nanotechnol.* **2008**, *3*, 210−215.
(25) Huang, M.; Yan, H.; Chen, C.; Song, D.; Heinz, T. F.; Hone, J. Phonon Softening and Crystallographic Orientation of Strained Graphene Studied by Raman Spectroscopy. *Proc. Natl. Acad. Sci. U.S.A.* **2009**, *106*, 7304−7308.
(26) Corro, E. D.; Taravillo, M.; Baonza, V. G. Nonlinear Strain Effects in Double-Resonance Raman Bands of Graphite, Graphene, and Related Materials. *Phys. Rev. B* **2012**, *85*, No. 033407.
(27) Wu, Y.; Zhai, D.; Pan, C.; Cheng, B.; Taniguchi, T.; Watanabe, K.; Sandler, N.; Bockrath, M. Quantum Wires and Waveguides Formed in Graphene by Strain. *Nano Lett.* **2018**, *18*, 64−69.
(28) Kasry, A.; Ardakani, A. A.; Tulevski, G. S.; Menges, B.; Copel, M.; Vyklicky, L. Highly Efficient Fluorescence Quenching with Graphene. *J. Phys. Chem. C* **2012**, *116*, 2858−2862.
(29) Ajayi, O. A.; Anderson, N. C.; Cotlet, M.; Petrone, N.; Gu, T.; Wolcott, A.; Gesuele, F.; Hone, J.; Owen, J. S.; Wong, C. W. Time-Resolved Energy Transfer from Single Chloride-Terminated Nanocrystals to Graphene. *Appl. Phys. Lett.* **2014**, *104*, No. 171101.
(30) Raja, A.; Montoya-Castillo, A.; Zultak, J.; Zhang, X.-X.; Ye, Z.; Roquelet, C.; Chenet, D. A.; van der Zande, A. M.; Huang, P.; Jockusch, S.; Hone, J.; Reichman, D. R.; Brus, L. E.; Heinz, T. F. Energy Transfer from Quantum Dots to Graphene and $MoS_2$: The Role of Absorption and Screening in Two-Dimensional Materials. *Nano Lett.* **2016**, *16*, 2328−2333.
(31) Liu, Y.; Liu, C. Y.; Liu, Y. Investigation on Fluorescence Quenching of Dyes by Graphite Oxide and Graphene. *Appl. Surf. Sci.* **2011**, *257*, 5513−5518.
(32) Kim, H.-J.; Sung, J.; Chung, H.; Choi, Y. J.; Kim, D. Y.; Kim, D. Covalently Functionalized Graphene Composites: Mechanistic Study of Interfacial Fluorescence Quenching and Recovery Processes. *J. Phys. Chem. C* **2015**, *119*, 11327−11336.
(33) Gonçalves, H.; Bernardo, C.; Moura, C.; Ferreira, R. A. S.; Andre, P. S.; Stauber, T.; Belsley, M.; Schellenberg, P. Long Range Energy Transfer in Graphene Hybrid Structures. *J. Phys. D: Appl. Phys.* **2016**, *49*, No. 3315102.
(34) Walker, B.; Port, H.; Wolf, H. C. The Two-Step Excimer Formation in Perylene Crystals. *Chem. Phys.* **1985**, *92*, 177−185.
(35) Nishimura, H.; Yamaoka, T.; Mizuno, K.; Iemura, M.; Matsui, A. Luminescence of Free and Self-trapped Excitons in $\alpha$ and $\beta$-Perylene Crystals. *J. Phys. Soc. Jpn.* **1984**, *53*, 3999−4008.
(36) Pick, A.; Klues, M.; Rinn, A.; Harms, K.; Chatterjee, S.; Witte, G. Polymorph-Selective Preparation and Structural Characterization of Perylene Single Crystals. *Cryst. Growth Des.* **2015**, *15*, 5495−5504.
(37) Fujino, T.; Tahara, T. Femtosecond Fluorescence Up-Conversion Microscopy: Exciton Dynamics in $\alpha$-Perylene Microcrystal. *J. Phys. Chem. B* **2003**, *107*, 5120−5122.
(38) Ishino, H.; Iwai, S.; Iwamoto, S.; Okumura, T.; Nishimoto, T.; Nair, S. V.; Kobayashi, T.; Tokunaga, E. Absorption and Emission Spectra of Molecular Excitons in Single Perylene Nanocrystals. *Phys. Rev. B: Condens. Matter Mater. Phys.* **2011**, *84*, No. 041303.
(39) Swathi, R. S.; Sebastian, K. L. Long Range Resonance Energy Transfer from a Dye Molecule to Graphene has $(\text{Distance})^{-4}$ Dependence. *J. Chem. Phys.* **2009**, *130*, No. 086101.
(40) Wang, Y.; Kurunthu, D.; Scott, G. W.; Bardeen, C. J. Fluorescence Quenching in Conjugated Polymers Blended with Reduced Graphitic Oxide. *J. Phys. Chem. C* **2010**, *114*, 4153−4159.
(41) Gaudreau, L.; Tielrooij, K. J.; Prawiroatmodjo, G. E. D. K.; Osmond, J.; de Abajo, F. J. G.; Koppens, F. H. L. Universal Distance-Scaling of Nonradiative Energy Transfer to Graphene. *Nano Lett.* **2013**, *13*, 2030−2035.



DOI: 10.1021/acsomega.8b00872
*ACS Omega* 2018, 3, 8129−8134